Preprint Title Effect of Ag Loading Location on the Photocatalytic Performance of a TiO_2 Nanocolumn Array

Authors Jinghan Xu, Yan Zhao and Yanqi Liu

Publication Date 26 Sep 2019

Article Type Full Research Paper

ORCID® iDs Jinghan Xu - https://orcid.org/0000-0002-4031-9644; Yan Zhao - https://orcid.org/0000-0003-1177-7600

Effect of Ag Loading Location on the Photocatalytic Performance of a TiO_2 Nanocolumn Array

Jinghan Xu[1,2], Yan Zhao[1,2*] and Yanqi Liu[1,2]

[1]Beijing Engineering Research Center of Laser Technology, Research Institute of Laser Engineering, Beijing University of Technology, No. 100 Pingle Park, Chaoyang District, Beijing 100124, People's Republic of China

[2]Key Laboratory of Trans-scale Laser Manufacturing Technology, Ministry of Education，, Research Institute of Laser Engineering, Beijing University of Technology, No. 100 Pingle Park, Chaoyang District, Beijing 100124, People's Republic of China

Correspondence author

E-mail: zhaoyan@bjut.edu.cn

Abstract

The evaluation of the photocatalytic performance of Ag-loaded TiO_2 nanocolumn (Ag-TNC) arrays prepared by atomic layer deposition (ALD) and vacuum evaporation is described. The effects of Ag loading position and deposition thickness on the morphology, structure, composition, and optical and photocatalytic properties of the Ag-TNC arrays were studied by controlling the preparation process and vacuum evaporation time. The Ag-filled samples were found to maintain high catalytic efficiency, whereas that of the Ag-coated samples decreased with the increase of Ag deposition thickness. The reasons for the influence of the loading position on the catalytic efficiency are discussed, and the conclusions were verified by simulation.

Keywords: Ag, TiO_2, nanoarray, heterojunction, photocatalytic

1. Introduction

Since 1972, when Shimada and Honda discovered the photocatalysis of titanium dioxide (TiO_2) under ultraviolet light (UV), research in this field has never stopped growing [1]. Recently, TiO_2 has been utilized in the fields of photocatalytic water decomposition [2], photocatalytic organic degradation [3], and artificial photosynthesis [4]. In particular, research on the application of TiO_2 in the field of water pollution degradation has experienced a notable increase due to its nontoxicity, nonpollutant nature, high chemical stability, and low price [5]. However, the absorption spectrum of pure TiO_2 is too narrow (200–400 nm), and the high hole–electron pair recombination rate restricts its photocatalytic efficiency [6,7].

Many efforts have been devoted to solve these problems with the aim of improving the catalytic performance of TiO_2, which include doping with nonmetal elements [8], dye sensitization [9], and combination with metal elements or other metal oxides [10]. Compared with the bulk material, one-dimensional (1D) nanostructured TiO_2 presents enhanced photocatalytic activity that depends on a variety of factors such as surface area, particle shape, crystalline structure, crystal size, and surface active sites [11,12]. In addition, the combination of nanostructured TiO_2 with a precious metal to form a metal–oxide structure has been shown to greatly improve the catalytic efficiency of the material [13]. At present, the preparation of 1D TiO_2 nanostructures is mainly performed by using anodization [14] and

hydrothermal [15] and template [16] methods. Meanwhile, the most common methods for the combination with precious metals are chemical deposition [17] and physical deposition [18].

The development of anodized aluminum oxide template (AAO) constituted an important advance in the field of film preparation, since it allows the formation of nanostructured films with high degree of morphology control [19]. Furthermore, according to Das et al. [20], the use of atomic layer deposition (ALD) for the preparation of TiO_2 films affords specimens with different electron transfer characteristics than those of rutile and anatase TiO_2, and the as-prepared films fit the template well. When Ag particles are combined with TiO_2, the photocatalytic performance of the film can be significantly enhanced by hot electron injection [21], localized surface plasmon resonance (LSPR) [22], and plasma excitation light scattering [23,24]. Cushing et al. [25] used the time-resolved method to track these three processes by establishing a density matrix model, which allowed them to predict the theoretical maximum catalytic efficiency and theoretical optimal structure of the plasma metal–semiconductor heterojunction. Having this background in mind, we decided to prepare a TiO2 nanocolumn (TNC) structure by using AAO in combination with ALD, in which Ag particles could be selectively supported separately outside and inside the nanocolumns.

Most of the 1D TiO_2-Ag nanostructures prepared to date are Ag

nanoparticle-coated TiO_2 (ACT), in which the catalytic efficiency of the catalyst is greatly decreased when the Ag loading is increased to a certain extent. Wang et al. [26] used the hydrothermal method to prepare an array of TiO_2 nanocolumns, whose outside surface was then coated with Ag particles by chemical deposition. After seven depositions, the catalytic efficiency of the as-prepared TiO_2-Ag film decreased significantly. A similar decline in catalytic efficiency was observed in a TiO_2 nanocolumn array fabricated by photolithography and template method by Sung [27]. In this case, Ag particles were loaded outside the nanocolumns by magnetron sputtering, and the catalysis was carried out at a sputtering time of 30 min. Besides, Jani et al. [28] studied the preparation of TiO_2 nanotube arrays by anodization, and Ag particles were loaded inside and outside the nanotubes by chemical deposition. The catalysis of this composite was carried out at a concentration of 1100 Mm in $AgNO_3$ solution. It was found that the loading position of precious metal particles in the TiO_2 structure could not be regulated, which had a negative effect on the catalytic efficiency. For these reasons, we considered it worthwhile to study the effect that the position of the Ag loading may have on the catalytic efficiency of the newly prepared Ag-loaded TiO_2 nanocolumn (Ag-TNC) arrays.

2. Experimental

Aluminum sheets, chromic acid (H_2CrO_4), and methylene blue (MB) were

purchased from Alfa Aesar. Alcohol, perchloric acid ($HClO_4$), and sulfuric acid (H_2SO_4) were purchased from Beijing Chemical Works. All the chemicals used in the experiments were of analytical grade and used without further purification.

2.1 Method

Anodized aluminum template preparation: Highly pure aluminum sheets (purity > 99.9%, 20 × 20 × 0.5 mm) were subjected to secondary anodization to prepare highly ordered AAO templates. Thus, each aluminum sheet was annealed prior to oxidation and then electrochemically polished using a 1:4 volume ratio of $HClO_4$ and alcohol. The anodized electrolyte solution was 0.2 M H_2SO_4, the oxidation voltage was 20 V, the ambient temperature was maintained at 0 °C, and the oxidation time was 6 h. After the oxidation was completed, the aluminum sheet was immersed in 1.8 wt% H_2CrO_4 to remove the first oxide layer. The sample was then subjected to second oxidation under the same conditions as the first oxidation. After an oxidation time of 60 s, a single-pass AAO template with a pore diameter of 40 nm, a pore pitch of 65 nm, and a pore depth of 150 nm was obtained.

Ag-TNC array preparation: An array of TiO_2 nanocolumns was deposited (300 cycles) on the AAO template using ALD (homemade) with $TiCl_4$ as the precursor.

The preparation of Ag-filled TiO_2 nanocolumns (AFT) was as follows:

A sample deposited with TiO_2 was placed in a vacuum evaporation apparatus (Shen Yang, LN-1004A) and subjected to Ag deposition at a deposition pressure of 10^{-4} Pa, an evaporation source current of 44 A, and an evaporation rate of 0.08 nm/s. The sample was then transferred onto a crystal adhesive, and the AAO was removed by immersing the sample in 0.2 M NaOH solution for 24 h to obtain the Ag-TiO_2 array.

For the preparation process of Ag-coated TiO_2 nanocolumns (ACT), the Ag deposition was performed after removal of the AAO template as follows: The sample deposited with TiO_2 was supported onto crystal adhesive and then immersed in 0.2 M NaOH solution to remove residual Al and AAO. Then, the sample was cleaned, dried, and placed in a vacuum evaporation apparatus for deposition of Ag particles under the same conditions described above.

Table 1 summarizes the samples and preparation conditions, and a schematic of the preparation process is shown in Fig. 1.

2.2 Characterization

The surface and cross-sectional morphology of the Ag-TNC were observed using a field emission scanning electron microscope (FE-SEM, FEI, Tecnai G2 F30). The elemental composition and valence distribution of the film were measured by X-ray photoelectron spectroscopy (XPS, Thermo Fisher Scientific, ESCALAB 250Xi). The photoluminescence (PL) intensity of the array was measured using a laser of 325 nm excitation

wavelength and a grating spectrometer (Horiba, JY iHR550). The diffuse reflectance absorption spectrum of the array was measured using an ultraviolet–visible spectrophotometer (UV–vis, Shimadzu, UV-3600).

Photocatalytic experiments. The photocatalysis was performed under 300 W Xe light using 15 mL of a 5 ppm MB solution. Before starting the photocatalysis, the sample was immersed in the MB solution and allowed to stand in the dark for 30 minutes to reach the adsorption–desorption balance. Then, the solution was placed under a light source to start the photocatalysis. Every 10 min, an aliquot of 2 mL was transferred into a UV–vis cuvette, and the change in absorbance was measured using a UV–vis spectrophotometer (Shimadzu, UV-3600). After the measurement was completed, the solution was poured back into the beaker to keep the total volume unchanged.

Table 1

Summary of the preparation conditions of Ag-loaded TiO_2 samples

Sample code	**Scheme name**	**Deposition time (Ag)**	**Deposition thickness (Ag)**
TNC	TiO_2 NC	0	0
AFT1	Ag-filled TiO_2 NC	250 s	10 nm
AFT2	Ag-filled TiO_2 NC	500 s	20 nm
AFT3	Ag-filled TiO_2 NC	1000 s	40 nm

ACT1	Ag-coated TiO_2 NC	250 s	10 nm
ACT2	Ag-coated TiO_2 NC	500 s	20 nm
ACT3	Ag-coated TiO_2 NC	1000 s	40 nm

3. Result and discussion

Fig. 1 depicts a schematic diagram of the preparation process of the ACT and AFT nanocolumn arrays (schemes (1) and (2), respectively). In the structure represented in (2), the bottom of the array hinders the dense accumulation of Ag nanoparticles in the nanocolums or the formation of agglomerates. Instead, the Ag-filled TiO_2 nanocolumn structure (2) is obtained. On the other hand, the Ag-coated structure (1) is formed without the hindrance of the bottom structure, in which the Ag nanoparticles deposit more densely and form larger nanoparticles. The structural differences between the ACT and AFT arrays depicted in (1) and (2) can be invoked as the main reason for the differences observed in their physical and catalytic properties, which will be discussed later.

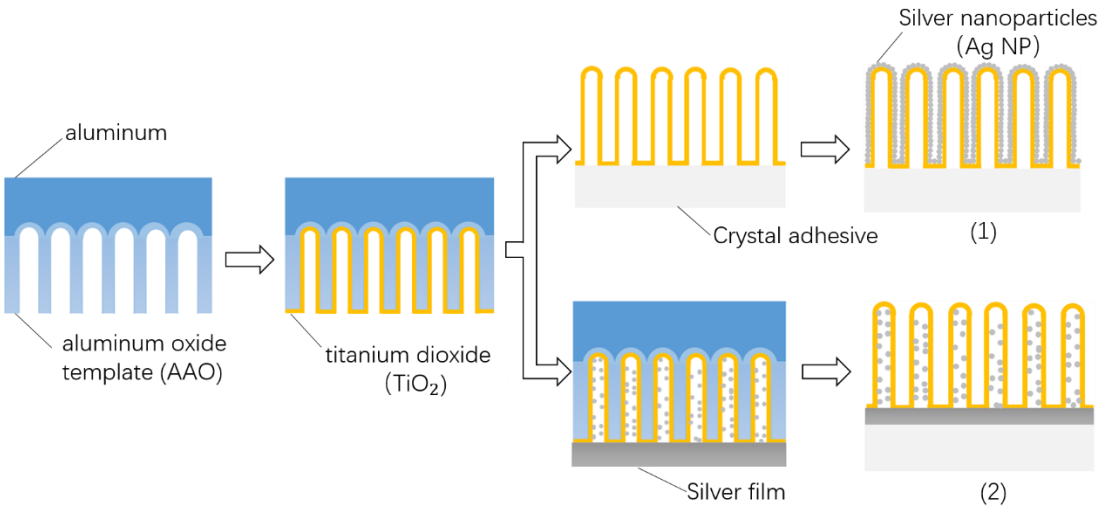

Figure 1. Schematic diagram of the preparation process of the different Ag-TiO_2 NC structures. (1) Structure of samples ACT1, ACT2, and ACT3; (2) structure of samples AFT1, AFT2, and AFT3.

Fig. 2 shows SEM images of the top view of all samples and elemental composition of TNC, from which the effects of different Ag deposition thicknesses and cladding structures can be observed. Fig. 2a and 2b shows the morphology of the prepared AAO template and the TiO_2 nanocolumn array prior to the Ag deposition, respectively. As can be seen, ALD perfectly replicates the template structure. Fig. 2c is the EDS spectrum of TNC, and we can find that the elements of the array are mainly composed of C, O, and Ti. Among them, C comes from organic substrates. Fig. 2d, 2e, and 2f are AFT structures with thickness of Ag deposition of 10, 20, and 40 nm, respectively. From the observation of these figures, it can be concluded that the deposition of Ag does not affect the structure of TiO_2, and the array of nanocolumns is well preserved and consistent with the deposition. Meanwhile, Fig. 2g, 2h, and 2i show the ACT structures, which exhibit Ag deposition thicknesses of 10, 20, and 40 nm, respectively. We can see that, as the thickness of Ag deposition increases, the array of TiO_2

is gradually covered until the nanocolumn structure disappears.

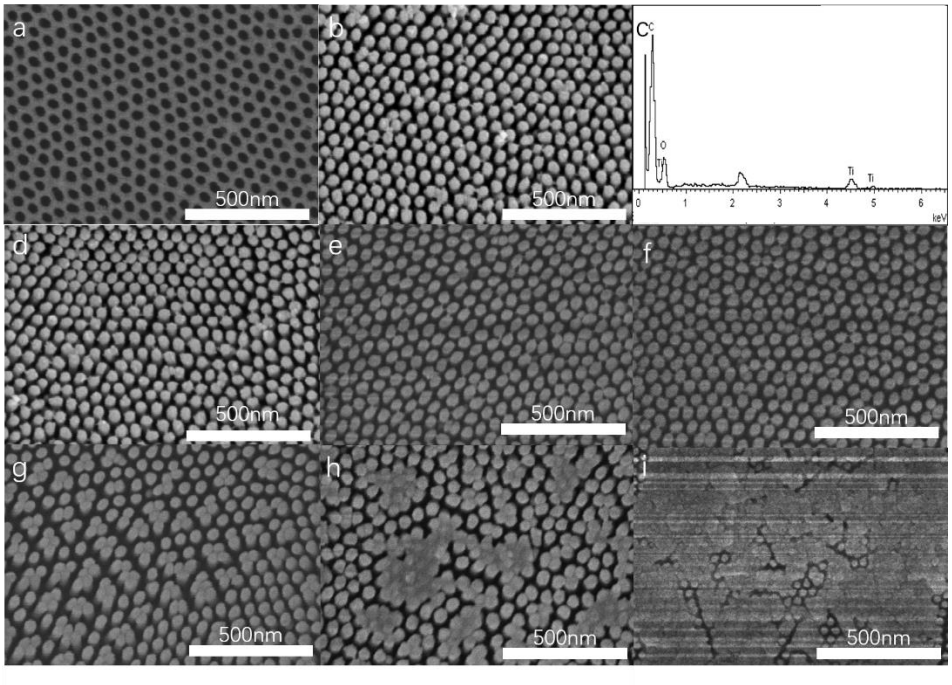

Figure 2. SEM images of the top view of different samples: (a) AAO template, (b) TNC, with a sectional view of TNC in the inset, (c) AFT1, (d) AFT2, (e) AFT3, (f) ACT1, (g) ACT2, and (h) ACT3.

To observe the distribution of Ag nanoparticles in the AFT nanocolumn array, the AAO template was broken by bending the samples prior to removal of Al and AAO, exposing the internal structure of the nanocolumn as shown in Fig. 3. Fig. 3a shows how to observe the cross section of the sample. Fig. 3b is the cross section of the AAO template, and we can find that there is nothing to cover the surface of the template. Fig. 3c is the cross section of TNC sample. Comparing Figures 3b and c, we can find that TiO_2 perfectly covers the surface of AAO, the nanocolumn is hollow structure, and the top hole still exists. As can be seen from Fig. 3d, due to the low thickness of Ag deposition in AFT1, no obvious nanoparticles can be observed in the TNC array, and not much Ag aggregation is present around

the nanopore marked with the red circle, which means that Ag can still enter the nanocolumn easily. In contrast, Ag nanoparticles can be clearly seen on the inner wall of the TNC of AFT2 marked with the red circle in Fig. 3e. From the comparison of Fig. 3d and 3e, it can be concluded that the Ag particles deposited in the TNC become gradually larger, but no accumulation around the nanopores occurs, which would block further deposition of Ag particles. Finally, in the structure having the thickest layer of Ag (AFT3), a large amount of Ag accumulation can be observed around the nanopore marked with the yellow circle in Fig. 3f, which closes the nanopore and hinders excessive Ag deposition in the TNC. Comparing the areas marked with the red circles in Fig. 3e and 3f, it becomes apparent that the increase of Ag deposition thickness does not significantly increase the size and distribution density of the nanoparticles in the TNC, and that the Ag nanoparticles still exhibit appropriate size and good dispersion.

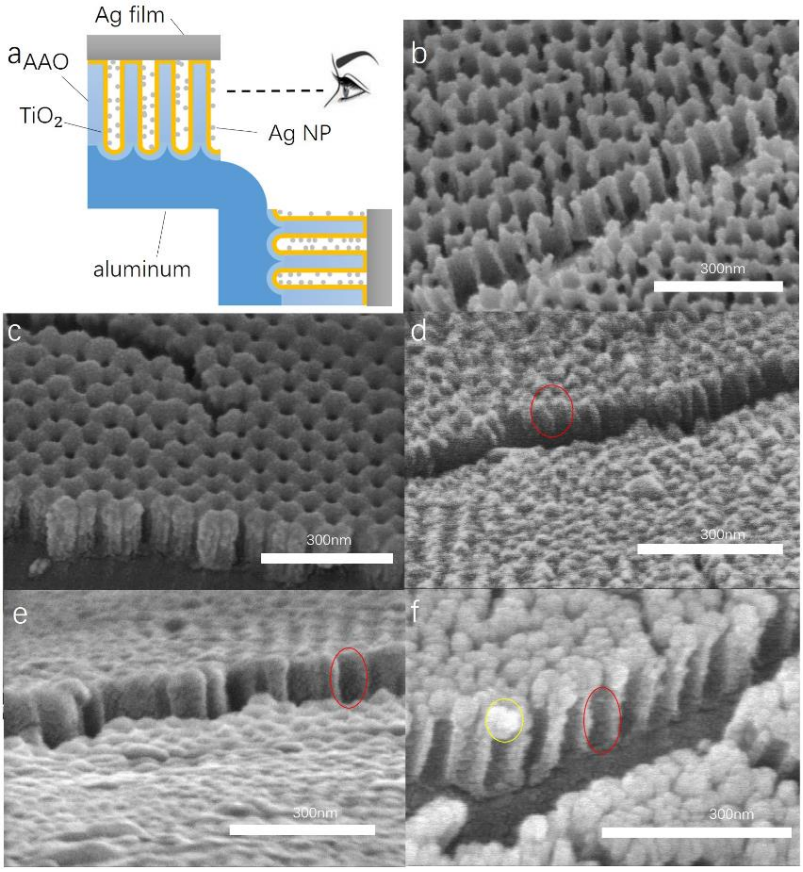

Figure 3. SEM cross section of samples with AAO and Al substrate. (a) Observation sketch, (b) AAO template, (c) TNC, (d) AFT1, (e) AFT2, and (f) AFT3.

Next, sample AFT3 was subjected to XPS analysis to characterize the elemental composition and chemical state of the Ag-TNC film, and the result is shown in Fig. 4. According to Fig. 4a, all the peaks can be attributed to Ti, O, C, and Ag, which indicates that the sample consists of TiO_2 and Ag. The appearance of the C element is attributable to contamination from the cavity of the XPS device and/or from the adhesive substrate. The high-resolution spectra of Ag, Ti, and O are shown in Fig. 4b, 4c, and 4d, respectively. In the spectrum of O 1s (Fig. 4b), the characteristic peak is observed at 531.8 eV. The shape of this peak is symmetrical, which is indicative of the presence of one distinct O species in the sample. Meanwhile, the two characteristic peaks of Ti 2p are located

at 458.6 and 464.3 eV in Fig. 4c. These peaks represent the binding energy of Ti 2p3/2 and Ti 2p1/2, which indicates that Ti is in the +4 valence state in the sample. The spacing between the two peaks of 5.7 eV is also consistent with the +4 oxidation state [29]. Fig. 4d shows the high-resolution spectrum of Ag. As can be seen from the figure, Ag 3d has two characteristic peaks at 367.5 and 373.5 eV, which are attributed to the binding energy of Ag 3d5/2 and Ag 3d3/2, with a spacing of 6 eV. This indicates that the structure of Ag in the sample is simple. Therefore, the results of the XPS analysis confirms that the sample is composed of TiO_2 and Ag.

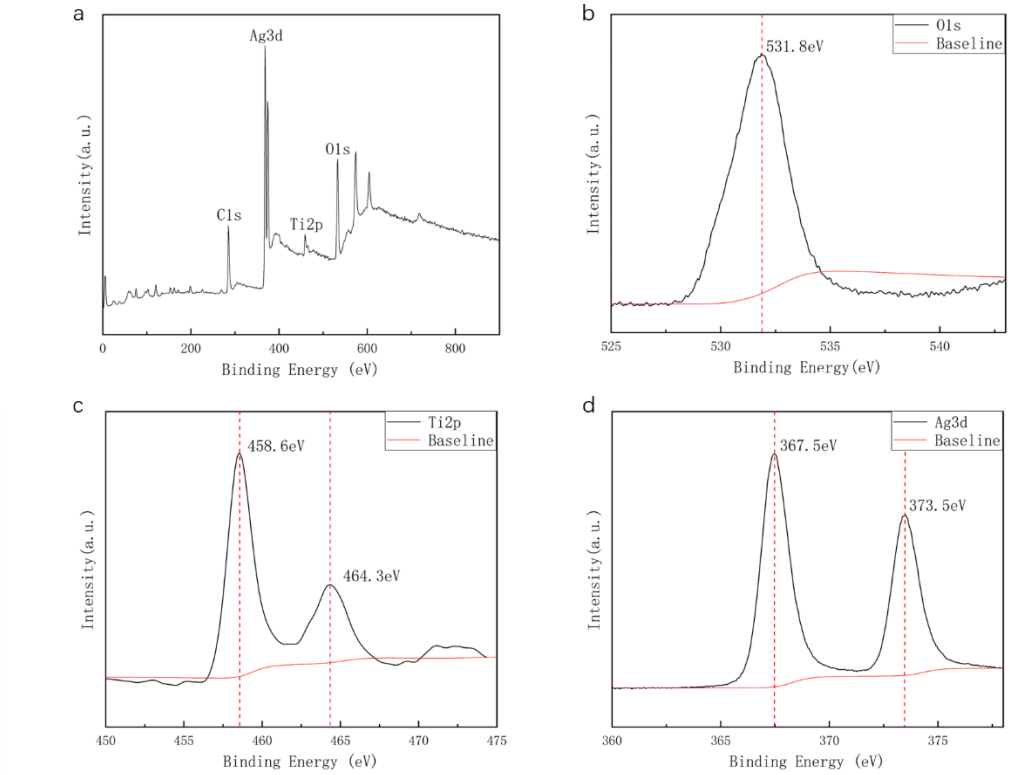

Figure 4. XPS spectrum of AFT3: (a) Survey, (b) O 1s, (c) Ti 2p, (d) Ag 3d.

In order to investigate the absorption properties of the different arrays,

the optical absorption tests of all samples were carried out, as shown in Fig. 5. Fig. 5(a) is the optical absorption spectra of TNC and AFT structure samples. It can be seen that the absorption peak of TiO_2 is located at 276nm and the absorption of the samples in the visible light portion increase as the thickness of Ag increases. Moreover, the increase of Ag thickness does not hinder the absorption of TiO_2 in the ultraviolet region. Fig. 5(b) is the optical absorption spectra of ACT structure samples. It can be seen that with the increase of Ag deposition, the visible absorption intensity of the samples increases gradually, but the absorption peak of TiO_2 at 276 nm decreases obviously. The absorption peak of ACT3 at 317 nm is the characteristic absorption peak of Ag prepared by vacuum evaporation, and the absorption peak at 364 nm is generated by the LPSR.[30]

Fig. 5c and d show the Tauc plots of the UV–vis spectra depicted in Fig. 5a and b, which are calculated using formula (1) for an indirect bandgap semiconductor, since the grains are small and the energy levels are discrete:

$$(\alpha h\nu)^{\frac{1}{2}} = A\left(h\nu - E_g\right) \quad (1)$$

In formula (1), h is Plank's constant (6.626×10^{-34} J s), ν is frequency of light, and Eg represents the band gap energy. For the calculation of E_g by the Tauc plot absorbance (Abs.) can be used directly instead of α; therefore, the E_g numerical value is determined by the intersection of the extension line and the x-axis(hν) [31]. It can be seen from Fig. 5c that the TiO_2 specimens prepared by ALD exhibit higher E_g (3.8 eV) than that obtained

using the conventional method (3.20 eV). This is attributed to the quantum size effect, according to which the E_g value of a semiconductor depends on physicochemical properties such as size, surface area, and crystalline phase [32]. When Ag particles are combined with TiO_2, the band gap of the resulting Ag-TNC film is narrowed under the action of LSPR and hot electron injection, and the samples have absorption peaks in the visible part. In fig. 5d, since Ag covers TiO_2, the light absorption of ACT3 is substantially generated by Ag, so the sample has no band gap.

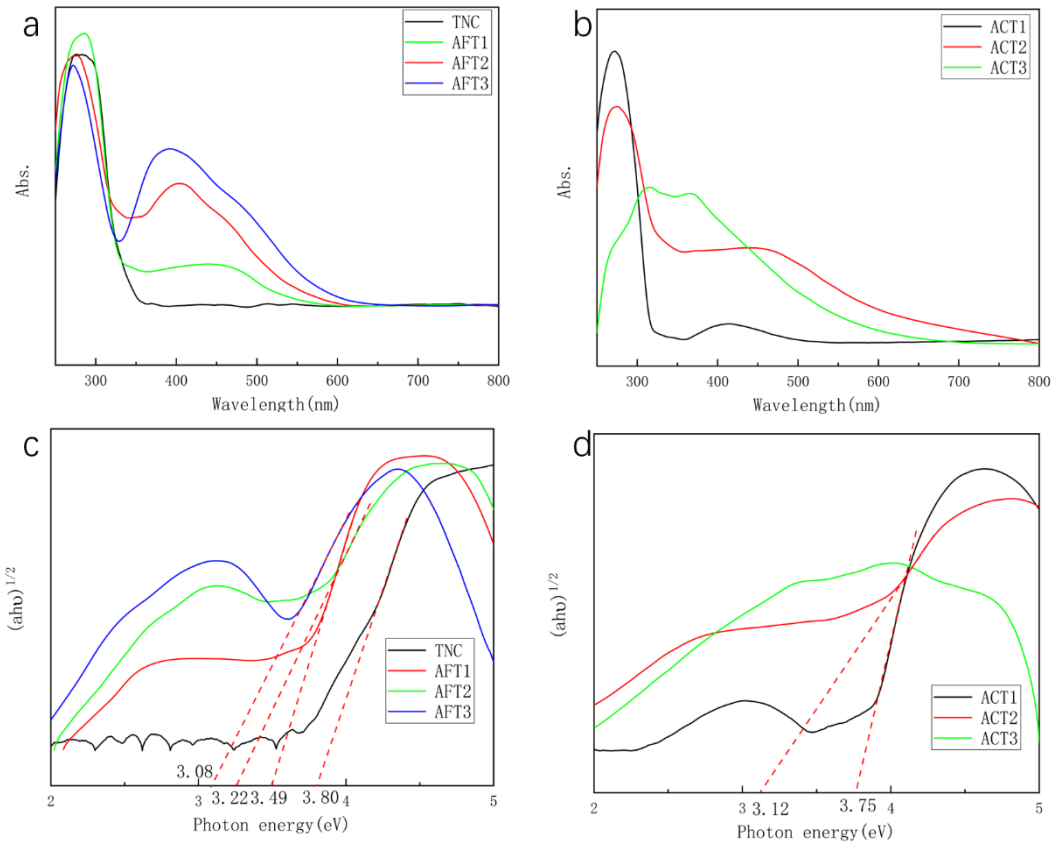

Figure 5. (a) UV–vis absorption spectra and (b) bandgaps of different samples.

To evaluate the influence of the different structures on the catalytic reaction, UV–vis photocatalytic experiments were carried out on different samples using MB solution as the reactant, as shown in Fig. 6. In these

experiments, the degradation efficiency can be described by the Lambert–Beer law and the Langmuir–Hinshelwood model as follows:

$$\mathrm{Abs.} = \mathrm{abC} \tag{2}$$

$$\eta = \frac{C_0 - C}{C_0} \times 100\% \tag{3}$$

$$\ln\left(\frac{C}{C_0}\right) = -K_\alpha \mathrm{t} \tag{4}$$

where Abs. is the solution absorbance, a is the solution absorbance coefficient, b is the optical path, C is the solution concentration, C_0 is the initial concentration, and K_α is the apparent first-order rate constant.

Fig. 6a shows that the AFT1 sample catalyzes the degradation of MB at different times. After 60 minutes of irradiation, the absorption intensity of MB at 663 nm substantially disappears, indicating that almost all the MB molecules are catalytically decomposed. Fig. 6c shows the degradation efficiency of different samples under Xe lamp illumination. It can be seen that the combination of Ag and TiO_2 results in a great improvement of the MB degradation efficiency. The Ag-TiO_2 specimens can achieve a decomposition rate of 96.9% after 60 min illumination, whereas TNC only reaches a decomposition rate of 71.4%. This is because the absorption light band of the sample is broadened in the presence of Ag particles. Under the same illumination conditions, more photogenerated carriers are generated in the Ag-TNC sample, and the transfer of the photogenerated electrons to the Ag particles reduces the recombination of electrons and holes, thereby increasing the number of electrons and holes involved in the catalytic

reaction. From the comparison of the Ag-loaded structures, it can be seen that AFT1 and ACT1 have very close catalytic efficiencies, indicating that the loading position does not affect the catalytic efficiency of the sample at low deposition thickness. In contrast, when the Ag deposition thickness increases, the catalytic efficiency of AFT remains unaltered, whereas that of ACT undergoes a significant decrease. This decrease is further evidenced in Fig. 6b, in which the K_α from formula (3) of samples ACT1, ACT2, and ACT3 gradually decreases, and specific K_α values are shown in Table 2. Fig. 6d shows the stability of samples ACT3 and AFT3, where it can be seen that, after repeating the photocatalytic process five times, both samples maintain an efficiency close to the first catalytic cycle. This result indicates that the samples prepared by the combination of ALD and vacuum evaporation have good stability, which is not affected by the different loading structures, i.e., Ag-coated or -filled.

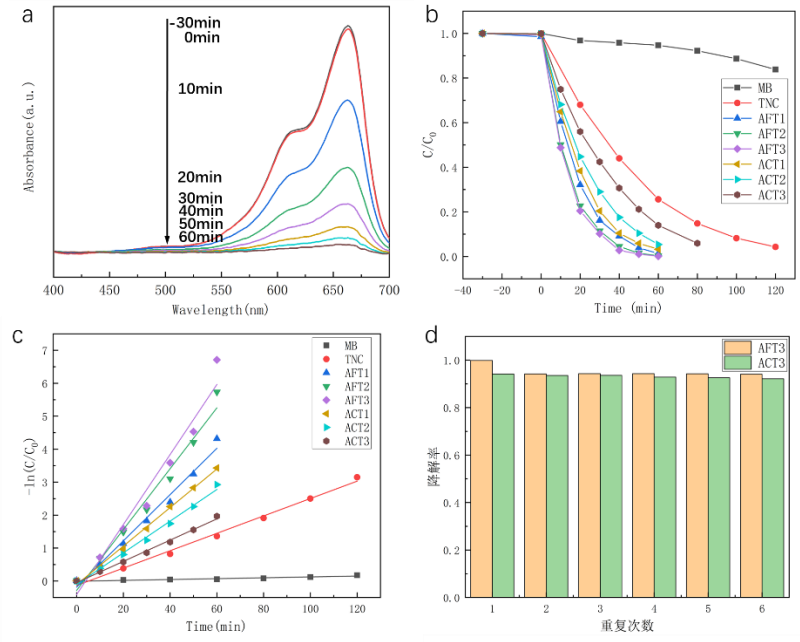

Figure 6. Photocatalytic activity for the degradation of MB: (a) UV–vis absorption spectra for the photocatalytic degradation of MB in the presence of AFT1 sample, (b) photocatalytic degradation rate of MB by different samples and pure MB under UV–vis light, (c) kinetics of different samples, (d) recycling of AFT3 and ACT3.

Table 2
Summary of Kinetic Constants of Photocatalytic Reaction

Sample code	Kinetic constants of chemical reactions (K_α)
TNC	0.0264
AFT1	0.0702
AFT2	0.0923
AFT3	0.1064
ACT1	0.0685
ACT2	0.0481
ACT3	0.0322

In order to elucidate the mechanism of the influence of Ag loading position and deposition thickness on the photocatalytic reaction, we used Finite-Difference Time-Domain (FDTD) simulation to study the electromagnetic field distribution of Ag-loaded TiO_2 arrays with different structures. Fig.7 is the simulation of the electric field distribution of arrays with different structures at 457 and 320 nm. In order to further illustrate the effect of structural changes on the electric field distribution of arrays, the XY plane and the XZ plane are chosen to analyze the arrays. The XY plane chooses the cross section at 75 nm and the XZ plane chooses the cross section at 0 nm. The structure of the model was established according to the morphology observed by SEM.As can be seen from the figure 7 (a1-

4), the electric field of the TiO_2 arrays is stronger under 320 nm illumination, and there is a strong electric field distribution between the nanocolumns at the altitude of 50-120 nm. Figure 7 (b1-4) are simulations of ACT3 structure. Ag was filled between the nanocolumns, and a layer of 15 nm thick Ag film was covered on the top of the array. It can be seen from the figure that Ag coating hinders the absorption of ultraviolet light by TiO_2, and the electric field intensity between nanocolumns decreases obviously. Only under 457 nm light, there is a strong electric field distribution at the top of the array, which is attributed to the absorption of visible light by the LSPR resonance of Ag. Fig 7 (c1-4) is the simulation of the AFT3 structure. The diameter of Ag particles in the nanocolumn is 8 nm, the distance between the horizontal and vertical spherical centers is 11 nm, the distance between the vertical spherical centers is 14 nm, and the diameter of Ag particles at the bottom of the nanocolumn is 15 nm. At the same time, the bottom of the nanocolumn is covered with an Ag film of 15 nm thickness. It can be seen from the figure that under 457 nm illumination, due to the LSPR effect of Ag particles, strong electric field is generated on Ag particles, and hot electrons are injected intoTiO_2, so the electric field intensity at the interface between Ag and TiO_2 is the highest.

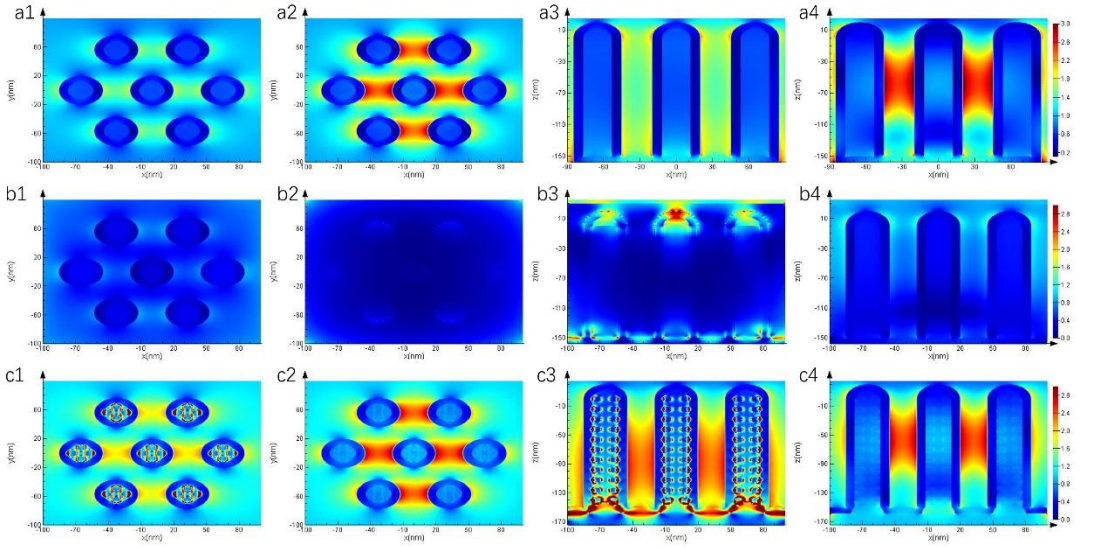

Figure. 7 FDTD simulates the electric field distribution of Ag-loaded TiO_2 nanocolumns with different structures. a1) wavelength 457 nm TNC cross section, a2) wavelength 320 nm TNC cross section, a3) wavelength 457 nm TNC longitudinal section, a4) wavelength 320 nm TNC longitudinal section, b1) wavelength 457 nm ACT3 cross section, b2) wavelength 320 nm ACT3 cross section, b3) wavelength 457 nm ACT3 longitudinal section, b4) wavelength 320 nm ACT3 longitudinal section, c1) wavelength 457 nm AFT3 cross section, c2) wavelength 320 nm AFT3 cross section, c3) wavelength 457 nm AFT3 longitudinal section, c4) wavelength 320 nm AFT3 longitudinal section.

Fig. 8a shows the photoelectric energy conversion of Ag-TiO_2 structure. The contact between Ag and n-type semiconductor TiO_2 will form Schottky barrier at the interface, which results in the bending of the energy band of TiO_2. [33] Due to the influence of SPR and LSPR effects, Ag can absorb visible light and make the electron near Fermi level transit to higher level. [34] When the high-level electrons have enough energy, the electrons will cross the Schottky barrier, transfer to the conduction band of TiO_2, or directly participate in the catalytic reaction. [35] Because of the wide band gap, TiO_2 can only absorb UV light. After the valence band electron absorbs photon energy, it transits from valence band to conduction band, and takes part in the catalytic reaction with the electrons transferred from

Ag. In the recombination process, the conduction band electrons which are not involved in the catalytic reaction can occupy the impurity level near the Fermi level and transfer to Ag to participate in the energy conversion process again. At the same time, the light and heat generated by the recombination process can also be absorbed by Ag, thus increasing the concentration of photogenerated electrons and the rate of catalytic reaction. [36] However, when Ag covered with TiO_2, Ag blocked the absorption of ultraviolet light by TiO_2, resulting in the absence of photogenerated carriers. Only the energetic electrons produced by Ag could participate in the catalytic reaction, as shown in Fig. 8c.

In Fig. 8b and d, a schematic diagram of the energy conversion of the two different nanocolumn structures is shown. In the AFT structure, the good transmittance of TiO_2 to visible light ensures that the absorption of visible light by Ag will not be hindered.[37] Conversely, in the ACT structure, Ag will over occupy the active site of TiO_2 [38], which hinders the absorption of photons by TiO_2 and the contact with MB molecules [39], affecting the catalytic reaction. In addition, since the chemical transformation of MB molecules occurs at the Ag-TiO_2 interface, Ag is more easily oxidized, which damages the long-term stability of the Ag-TiO_2 heterojunctions [40]. Taken together, these factors can explain the difference of catalytic efficiency between AFT and ACT.

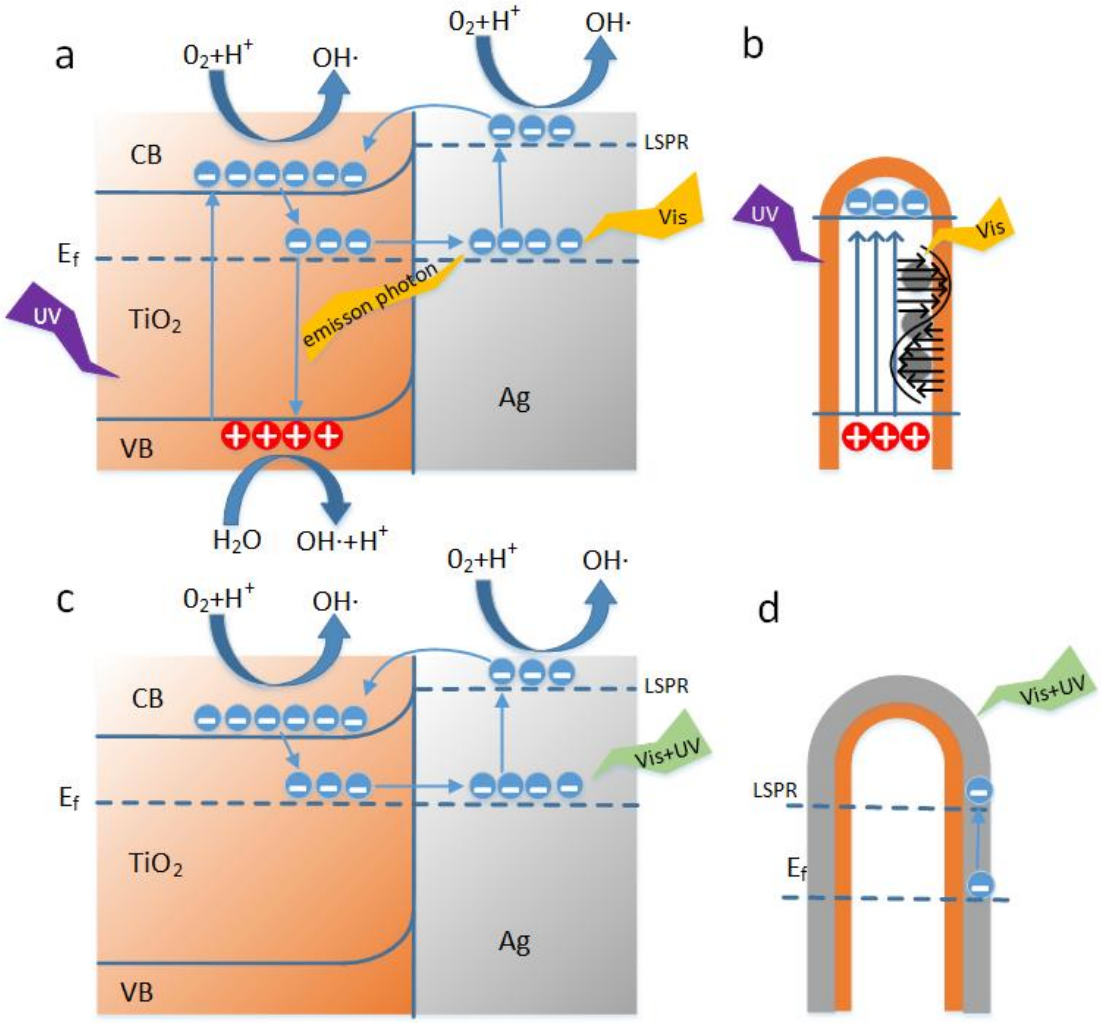

Figure 8. (a) Schematic diagram of electron–hole separation and energy conversion of Ag–TiO_2 structure under UV–Vis illumination. b) AFT structure light absorption diagram, c) schematic diagram of energy conversion when excessive Ag coated TiO_2, d) ACT structure light absorption diagram.

4. Conclusion

By combining the interaction mechanism between noble metal particles and semiconductor materials by template method, the effect of different loading positions of Ag particles on the catalytic efficiency of Ag-loaded TiO_2 nanocolumn (Ag-TNC) arrays has been evaluated. According to the results of photocatalytic experiments, the presence of Ag particles can improve the catalytic efficiency of the TNC structure, but the increase of Ag deposition thickness reduces the catalytic efficiency of the Ag-coated

TNC structure, evidencing the influence of loading location. The morphological analysis of ACT and AFT revealed that the size and distribution density of Ag particles in the ACT structure increase significantly with the deposition thickness, which weakens the LSPR effect. At the same time, the coating Ag particles hinder the absorption of light by TiO_2 and the contact with reactants, negatively affecting the catalytic reaction. In contrast, the excessive Ag deposition is limited by the special structure of the AFT samples, in which the absorption of visible light is not hindered. This can also be observed from the simulation results. Therefore, the catalytic efficiency of the AFT structure is not affected by the Ag deposition thickness and can always be maintained at a high level. In summary, the Ag-filled TiO_2 structure has more relaxed preparation parameters and stable catalytic efficiency than its Ag-coated counterpart, which renders it more applicable as a pollutant treatment material.

References

[1] Chen, X., & Mao, S. S. (2007). Titanium dioxide nanomaterials: synthesis, properties, modifications, and applications. Chemical reviews, 107(7), 2891-2959.

[2] Chen, X., Shen, S., Guo, L., & Mao, S. S. (2010). Semiconductor-based photocatalytic hydrogen generation. Chemical reviews, 110(11), 6503-6570.

[3] Asahi, R. Y. O. J. I., Morikawa, T. A. K. E. S. H. I., Ohwaki, T., Aoki, K., & Taga, Y. (2001). Visible-light photocatalysis in nitrogen-doped titanium oxides. science, 293(5528), 269-271.

[4] Li, M., Wang, M., Zhu, L., Li, Y., Yan, Z., Shen, Z., & Cao, X. (2018). Facile microwave assisted synthesis of N-rich carbon quantum dots/dual-phase TiO_2 heterostructured nanocomposites with high activity in CO2 photoreduction. Applied Catalysis B: Environmental, 231, 269-276.

[5] Ghosh, A., Nayak, A. K., & Pal, A. (2017). Nano-Particle-Mediated Wastewater Treatment: a Review. Current Pollution Reports, 3(1), 17-30.

[6] Tong, H., Ouyang, S., Bi, Y., Umezawa, N., Oshikiri, M., & Ye, J. (2012). Nano- photocatalytic materials: possibilities and challenges. Advanced materials, 24(2), 229-251.

[7] Diebold, U. (2003). The surface science of titanium dioxide. Surface science reports, 48(5-8), 53-229.

[8] He, H. Y., He, Z., & Shen, Q. (2018). TiO_2: Si nanotube/1T-MoSe2 nanosheet hybrids with highly efficient hydrogen evolution catalytic activity. Journal of colloid and interface science, 522, 136-143.

[9] Wang, X., Xiang, Y., Zhou, B., Zhang, Y., Wu, J., Hu, R., ... & Qu, J. (2019). Enhanced photocatalytic performance of Ag/TiO_2 nanohybrid sensitized by black phosphorus nanosheets in visible and near-infrared light. Journal of colloid and interface science, 534, 1-11.

[10] Fang, W., Xing, M., & Zhang, J. (2017). Modifications on reduced titanium dioxide photocatalysts: A review. Journal of Photochemistry and Photobiology C: Photochemistry Reviews, 32, 21-39.

[11] Zhukovskii, Y. F., Piskunov, S., Lisovski, O., Bocharov, D., & Evarestov, R. A. (2017). Doped 1D Nanostructures of Transition- metal Oxides: First- principles Evaluation of Photocatalytic Suitability. Israel Journal of Chemistry, 57(6), 461-476.

[12] Cheng, Z., Zhao, S., Han, Z., Zhang, Y., Zhao, X., & Kang, L. (2016). A novel preparation of $Ag@TiO_2$ tubes and their potent photocatalytic degradation efficiency. CrystEngComm, 18(45), 8756-8761.

[13] Liu, X., Iocozzia, J., Wang, Y., Cui, X., Chen, Y., Zhao, S., ... & Lin, Z. (2017). Noble metal–metal

oxide nanohybrids with tailored nanostructures for efficient solar energy conversion, photocatalysis and environmental remediation. Energy & Environmental Science, 10(2), 402-434.

[14] Yu, J., Dai, G., & Huang, B. (2009). Fabrication and characterization of visible-light-driven plasmonic photocatalyst Ag/AgCl/TiO_2 nanotube arrays. The Journal of Physical Chemistry C, 113(37), 16394-16401.

[15] Liu, B., & Aydil, E. S. (2009). Growth of oriented single-crystalline rutile TiO_2 nanorods on transparent conducting substrates for dye-sensitized solar cells. Journal of the American Chemical Society, 131(11), 3985-3990.

[16] Yao, Z., Wang, C., Li, Y., & Kim, N. Y. (2015). AAO-assisted synthesis of highly ordered, large-scale TiO_2 nanowire arrays via sputtering and atomic layer deposition. Nanoscale research letters, 10(1), 166.

[17] Wang, Q., Wang, X., Zhang, M., Li, G., Gao, S., Li, M., & Zhang, Y. (2016). Influence of Ag–Au microstructure on the photoelectrocatalytic performance of TiO_2 nanotube array photocatalysts. Journal of colloid and interface science, 463, 308-316.

[18] Dong, J., Ye, J., Ariyanti, D., Wang, Y., Wei, S., & Gao, W. (2018). Enhancing photocatalytic activities of titanium dioxide via well-dispersed copper nanoparticles. Chemosphere, 204, 193-201.

[19] Wen, L., Wang, Z., Mi, Y., Xu, R., Yu, S. H., & Lei, Y. (2015). Designing heterogeneous 1D nanostructure arrays based on AAO templates for energy applications. Small, 11(28), 3408-3428.

[20] Das, C., Richter, M., Tallarida, M., & Schmeißer, D. (2016). Electronic properties of atomic layer deposition films, anatase and rutile TiO_2 studied by resonant photoemission spectroscopy. Journal of Physics D: Applied Physics, 49(27), 275304.

[21] Govorov, A. O., Zhang, H., & Gun'ko, Y. K. (2013). Theory of photoinjection of hot plasmonic carriers from metal nanostructures into semiconductors and surface molecules. The Journal of Physical Chemistry C, 117(32), 16616-16631.

[22] Li, J., Cushing, S. K., Zheng, P., Meng, F., Chu, D., & Wu, N. (2013). Plasmon-induced photonic and energy-transfer enhancement of solar water splitting by a hematite nanorod array. Nature communications, 4, 2651.

[23] Awazu, K., Fujimaki, M., Rockstuhl, C., Tominaga, J., Murakami, H., Ohki, Y., ... & Watanabe, T. (2008). A plasmonic photocatalyst consisting of silver nanoparticles embedded in titanium dioxide. Journal of the American Chemical Society, 130(5), 1676-1680.

[24] Wu, N. (2018). Plasmonic metal–semiconductor photocatalysts and photoelectrochemical cells: a review. Nanoscale, 10(6), 2679-2696.

[25] Cushing, S. K., Bristow, A. D., & Wu, N. (2015). Theoretical maximum efficiency of solar energy conversion in plasmonic metal–semiconductor heterojunctions. Physical Chemistry Chemical Physics, 17(44), 30013-30022.

[26] Wang, X., Wang, Z., Jiang, X., Tao, J., Gong, Z., Cheng, Y., ... & Sun, Z. (2016). Silver-decorated TiO_2 nanorod array films with enhanced photoelectrochemical and photocatalytic properties. Journal of The Electrochemical Society, 163(10), H943-H950.

[27] Sung, D. I., Kim, H. G., Cha, S. K., Kim, D. H., Lee, H. B. R., Kim, S. O., ... & Yeom, G. Y. (2017). Photocatalytic effect of Ag/TiO_2 nanotubes fabricated using 40 nm-scale BCP lithography. Nanoscience and Nanotechnology Letters, 9(1), 50-55.

[28] Jani, N. A., Haw, C. Y., Chiu, W. S., Rahman, S. A., Lim, Y. C., Khiew, P. S., & Yaghoubi, A. (2017). Understanding the effect of plasmonic enhancement on photocatalytic activity of TiO_2 nanotube arrays. Materials Characterization, 128, 134-141.

[29] Yang, J., Jiang, Y. L., Li, L. J., Muhire, E., & Gao, M. Z. (2016). High-performance photodetectors and enhanced photocatalysts of two-dimensional TiO_2 nanosheets under UV light excitation. Nanoscale, 8(15), 8170-8177.

[30] Ji N, Ruan W, Li Z, et al. (2013). A potential commercial surface- enhanced Raman scattering–active substrate: stability and usability[J]. Journal of Raman Spectroscopy, 44(1): 1-5.

[31] Vijayalakshmi, R., & Rajendran, V. (2012). Synthesis and characterization of nano-TiO_2 via different methods. Archives of Applied Science Research, 4(2), 1183-1190.

[32] May-Lozano, M., Ramos-Reyes, G. M., López-Medina, R., Martínez-Delgadillo, S. A., Flores-Moreno, J., & Hernández-Pérez, I. (2014). Effect of the Amount of Water in the Synthesis of B-TiO_2: Orange II Photodegradation. International Journal of Photochemistry, 2014.

[33]Chuang H Y, Chen D H. (2011). Fabrication and photoelectrochemical study of Ag@ TiO_2 nanoparticle thin film electrode[J]. International Journal of Hydrogen Energy, 36(16): 9487-9495.

[34]Chen D, Chen Q, Ge L, et al. (2013). Synthesis and Ag-loading-density-dependent photocatalytic activity of Ag@ TiO_2 hybrid nanocrystals[J]. Applied Surface Science, 284: 921-929.

[35]Tan L L, Ong W J, Chai S P, et al. (2015). Noble metal modified reduced graphene oxide/TiO_2 ternary nanostructures for efficient visible-light-driven photoreduction of carbon dioxide into

methane[J]. Applied Catalysis B: Environmental, 166: 251-259.

[36]Zhang Z, Yates Jr J T. (2012). Band bending in semiconductors: chemical and physical consequences at surfaces and interfaces[J]. Chemical reviews, 112(10): 5520-5551.

[37] Zhang, Z., & Yates Jr, J. T. (2012). Band bending in semiconductors: chemical and physical consequences at surfaces and interfaces. Chemical reviews, 112(10), 5520-5551.

[38] Guan, H., Wang, X., Guo, Y., Shao, C., Zhang, X., Liu, Y., & Louh, R. F. (2013). Controlled synthesis of Ag-coated TiO_2 nanofibers and their enhanced effect in photocatalytic applications. Applied Surface Science, 280, 720-725.

[39] Subramanian, V., Wolf, E., & Kamat, P. V. (2001). Semiconductor−metal composite nanostructures. To what extent do metal nanoparticles improve the photocatalytic activity of TiO_2 films. The Journal of Physical Chemistry B, 105(46), 11439-11446.

[40] Devi, L. G., & Kavitha, R. (2016). A review on plasmonic metal TiO_2 composite for generation, trapping, storing and dynamic vectorial transfer of photogenerated electrons across the Schottky junction in a photocatalytic system. Applied Surface Science, 360, 601-622.